Hindawi
Advances in Materials Science and Engineering
Volume 2018, Article ID 7591576, 10 pages
https://doi.org/10.1155/2018/7591576

Research Article

Numerical Prediction of Chloride Penetration in Concrete Exposed to a Marine Environment at Tide

Sung In Hong and Ki Yong Ann

Department of Civil and Environmental Engineering, Hanyang University, Ansan 15588, Republic of Korea

Correspondence should be addressed to Ki Yong Ann; kann@hanyang.ac.kr

Received 21 December 2017; Accepted 29 March 2018; Published 24 April 2018

Academic Editor: Robert Cerný

Reinforced concrete structures under cyclic exposure to the corrosive environment such as the tidal zone as a part of marine structure entail the higher risk of steel corrosion. In this paper, chloride penetration in concrete exposed to the tidal zone was predicted using a combined moisture and chloride transport model. For the analysis of moisture transport, pore size distribution in concrete was determined from the experimental observation and used to determine the moisture permeability and degree of saturation. Then, the chloride profile through nonsaturated concrete cover was calculated by applying the moisture distribution along the penetration depth to the chloride convection and diffusion model. To assess sensitivity of the service life to the environment and concrete mix conditions, this study used three types of tide levels and water to cement ratios in the simulation. Under 10 years of tidal exposure condition, the minimum required cover depth at which the threshold chloride concentration reaches on the steel embedment increases only about 1.13 times as the tide level increases from the minimum to the highest while that for the w/c ratio increases about 1.69 times.

1. Introduction

The chloride-induced corrosion in RC structures especially exposed to marine environment has been regarded as a major problem in the aspect of structural safety. When a sufficient amount of chloride reaches on the steel surface in concrete, the passive film, maintained by high alkalinity of concrete pore solution, starts to dissolve and steel corrosion easily occurs [1]. After that, serial expansions of the corrosion products can cause concrete cracking from the location of steel embedment, thereby resulting in delineation of the concrete cover [2]. Thus, to assess the risk of chloride-induced corrosion and prevent the deterioration process during the life cycle of RC structures, a proper prediction model able to reflect the effects of material and environment actions on chloride ingress would be required.

Under the marine environment, the rate of chloride penetration in concrete largely depends on the exposure condition that changes with daily variation of the tide level [3]. Nevertheless, a number of studies for assessing the chloride ingress at the tidal zone with a single diffusion model have been carried out based on the assumption that the concrete pore network is fully saturated [3–6]. However, most of the concrete structures exposed to the tidal environment are in nonsaturated state, and the chloride transport is driven by both diffusion via concentration gradient through continuous pore water channel and convection via moisture movement through nonsaturated pores. In fact, as the exposure area becomes higher from the lowest tide level, chloride distribution in concrete becomes hard to be described with a single diffusion analysis since the moisture gradient in concrete simultaneously occurs during the repeated wet/dry cycles [7].

In the consideration of the transport mechanism in nonsaturated concrete, several prediction models have been developed [8–11]. Saetta et al. first suggested the S-shaped curve equation relating the chloride diffusivity with the moisture level to predict the chloride penetration under nonsaturated environment [8]. Based on this semiempirical expression of chloride diffusivity, the two-dimensional

numerical model for predicting temperature, relative humidity, and chloride transport in concrete was developed by Martin-Pérez et al. [9]. Nielsen and Geiker proposed the moisture dependent chloride diffusivity with a composite theory of the cement matrix to assess the chloride diffusion in nonsaturated state [10]. Recently, Sleiman et al. used the S-shaped curve relation of chloride diffusivity and moisture level to assess the effect of types of moisture adsorption isotherms on the ionic penetration in concrete [11]. However, moisture level at given humidity level largely changes with the concrete pore size distribution which also determines the moisture diffusivity as functions of humidity level and mix condition [12] and thus could affect the rate of chloride penetration in nonsaturated concrete.

The main topic in this study is to evaluate the dependences of tide level and the water to cement ratio on the chloride penetration using the combined moisture and chloride transport model. To implement the numerical calculation of the nonlinear transport behavior in the tidal zone, the finite element method (FEM) was adopted in solving the partial derivative equations with time-dependent boundary conditions. Moisture transport under the wet/dry cycles was modelled based on the statistical permeability theory to relate the pore size distribution in concrete to the moisture permeability. Then, chloride penetration in nonsaturated concrete can be predicted by applying the calculated spatial values of moisture transport to the chloride transport model.

2. Methodology

2.1. Moisture Transport. To predict the chloride transport in nonsaturated concrete, moisture distribution through the concrete depth was determined, considering the liquid and vapour transport which can be expressed as

$$\frac{\partial w}{\partial t} = \nabla\left(-K_{\mathrm{l}}\nabla P_{\mathrm{c}} + K_{\mathrm{v}}\nabla P_{\mathrm{v}}\right), \tag{1}$$

where w is the moisture content (kg/m^3), t is the time, K_{l} is the permeability of the liquid water (kg/m·s·Pa), P_{c} is the capillary pressure (Pa), K_{v} is the permeability of water vapour (kg/m·s·Pa), and P_{v} is the water vapour pressure (Pa). Assuming the thermodynamic equilibrium condition in concrete, it is possible to relate the pressure terms in (1) to the relative humidity (h) such that

$$\ln h = \ln\frac{P_{\mathrm{v}}}{P_0} = -\frac{P_{\mathrm{c}}M_{\mathrm{w}}}{\rho_{\mathrm{w}}RT}, \tag{2}$$

where P_0 is the saturation vapour pressure (Pa), ρ_{w} is the density of water (kg/m^3), R is the gas constant (J/kg·K), T is the temperature (K), and M_{w} is the water molecular weight (kg/mol). Thus, combining (1) and (2), moisture distribution in concrete in terms of relative humidity can be expressed as

$$\frac{\partial w}{\partial h}\cdot\frac{\partial h}{\partial t} = \nabla\left(K_{\mathrm{l}}\frac{\rho_{\mathrm{w}}RT}{M_{\mathrm{w}}h}\nabla h + K_{\mathrm{v}}P_0\nabla h\right), \tag{3}$$

where $\partial w/\partial h$ is the moisture storage capacity (kg/m^3), denoting the slope of water vapour isotherms for adsorption and desorption.

As the humidity level increases, the liquid permeability (K_{l}) increases due to the increase in the water content in concrete, while the vapour permeability (K_{v}) decreases due to the decrease in the nonsaturated porosity. K_{l} was determined based on the statistical permeability model [13], considering the probabilistic effect of the variation of pore sizes on the moisture flow in the porous cement matrix such that

$$K_{\mathrm{l}} = \frac{\rho_{\mathrm{w}}\varnothing^2}{8\tau^2\eta}\left(\int_0^{r_{\mathrm{c}}} r f(r)dr\right)^2, \tag{4}$$

$$\tau = -1.5\cdot\tanh\left[8.0\left(\varnothing - 0.25\right)\right] + 2.5, \tag{5}$$

$$f(r) = B\cdot\exp\left(-B\cdot r\right), \tag{6}$$

where $\varnothing$ is the porosity, τ is the tortuosity determined using a semiempirical model suggested by Nakarai et al. [14], η is the viscosity of liquid water (Pa·s), $f(r)$ is the normalized pore size distribution, B is the parameter of the Rayleigh–Ritz (R-R) density function, and r_{c} is the critical radius below which the pores are fully saturated (m), which can be expressed as

$$r_{\mathrm{c}} = t_{\mathrm{a}} + r_{\mathrm{k}}, \tag{7}$$

where t_{a} is the thickness of water molecules on the pore wall (m) and r_{k} is the capillary condensation radius (m). t_{a} can be determined according to the BET model [15] such that

$$t_{\mathrm{a}} = \frac{3\times10^{-10}\exp\left(855/T\right)}{(1-h)\left[1+\left(\exp\left(855/T\right)-1\right)h\right]}. \tag{8}$$

In the assumption of the cylindrical pore shape, r_{k} can be determined by using Kelvin's law such that

$$r_{\mathrm{k}} = -\frac{\delta\gamma M_{\mathrm{w}}}{\rho_{\mathrm{w}}RT}\cdot\frac{1}{\ln h}, \tag{9}$$

where δ is the constant dependent on the curvature of liquid-vapour interface [12, 15] and γ is the surface tension of water (N/m). For the simplicity of the analysis, change in δ during the moisture adsorption and desorption was not considered and assumed to be unity.

Before capillary condensation, adsorption of water molecules occurs through the nonsaturated pores, and the rate depends on the vapour permeability that can be described with the Knudsen diffusion model such that

$$K_{\mathrm{v}} = \frac{D_{\mathrm{v}}\left(1-S\right)}{\tau\left[1+l_{\mathrm{m}}/2\left(r_{\mathrm{m}}-t_{\mathrm{a}}\right)\right]}\left(\frac{M_{\mathrm{w}}}{RT}\right), \tag{10}$$

where S is the degree of saturation, l_{m} is the mean free path of the water molecule (m), r_{m} is the mean of pore radii over unsaturated pores (m) which was assume to be 2.5 μm equal to one-half of the maximum pore size, and D_{y} is the diffusion coefficient of water vapour in air (m^2/s), which was determined by taking into account the water vapour pressure and temperature differences [16] such that

$$D_v = D_{ref}\frac{P_{ref}}{P_v}\left(\frac{T}{T_{ref}}\right)^{1.88}, \quad (11)$$

where D_{ref} is the water vapour diffusivity at reference values of pressure (P_{ref}) and temperature (T_{ref}) ($D_{ref} = 21.6E-6\,m^2/s$, $P_{ref} = 11,325\,Pa$, and $T_{ref} = 273.16\,K$). In this study, the moisture content resulting from the vapour adsorption in nonsaturated pores was excluded due to its marginal influence on the chloride transport. Thus, the degree of saturation at wetting (S_w) was determined based on the pore size distribution such that

$$S_w = \int_0^{r_c} f(r)dr. \quad (12)$$

When vapour desorption proceeds, partial water contents remain through ink-bottle pores. By taking into account a probability of interconnection between larger pores and smaller at the given humidity level [13], the degree of saturation at drying (S_d) can be determined as

$$S_d = S_w\left(1 - \ln\left(S_w\right)\right). \quad (13)$$

When sea water contacts with the concrete surface, it was assumed that water vapour adsorption proceeds into the concrete cover, and the degree of saturation (S) was calculated with (12). When water vapour desorption proceeds from the inner concrete depth to the environment, the degree of saturation was calculated with (13).

2.2. Chloride Transport. Under the nonsaturated condition, chloride transport in concrete is driven by both diffusion via concentration gradient and convection via moisture flux. Considering the chloride binding during the combined ionic penetration, the mass balance equation for the chloride transport can be expressed as

$$\left(\frac{\partial C_b}{\partial C_f} + S\varnothing\right)\frac{\partial C_f}{\partial t} = \nabla\left(S\varnothing D_e \nabla C_f\right) + \nabla\left(S\varnothing C_f D_h \nabla h\right), \quad (14)$$

where C_b is the bound chloride concentration in concrete (kg/m^3), C_f is the free chloride concentration in pore solution (kg/m^3), D_e is the effective chloride diffusion coefficient (m^2/s), and D_h is the moisture diffusion coefficient (m^2/s) which accounts for the rate of combined liquid and vapour transport and can be obtained from (3) such that

$$D_h = \left(K_l\frac{\rho_w RT}{M_w h} + K_v P_0\right)\frac{\partial h}{\partial w}. \quad (15)$$

The Langmuir isotherm was used to describe a nonlinear relationship between free and bound chlorides. The derivative formula of the relation indicates the chloride binding capacity [9], which can be expressed as

$$\frac{\partial C_b}{\partial C_f} = \frac{\alpha}{\left(1 + \beta C_f\right)^2}, \quad (16)$$

where α and β are the binding parameters for the Langmuir isotherm.

Table 1: Boundary conditions for the moisture and chloride transport simulations.

Condition	Notation	Unit	Value
Wetting	h_{en}	—	0.995
	C_{en}	kg/m^3	17.75
Drying	h_{en}	—	0.7
	C_{en}	kg/m^3	0
Initial	H	—	0.995
	C_f	kg/m^3	0

2.3. Boundary Conditions. To mimic a typical tidal environment, three types of exposure conditions to the concrete surface were considered as low, medium, and high tide levels, corresponding to 0.3, 0.5, and 0.7 days of daily drying time, respectively. Accordingly, daily wetting time for the chloride ingress decreases from 0.7 to 0.3 days with increasing the tide levels. To do this, moisture and chloride fluxes into or out of the concrete surface were simulated using the following boundary conditions [8]:

$$\begin{aligned}\vec{n}\cdot\left(D_h\nabla h\right) &= B_h\left(h_s - h_{en}\right),\\ \vec{n}\cdot\left(D_e\nabla C_f\right) &= nB_c\left(C_s - C_{en}\right) + C_{en}B_h\left(h_s - h_{en}\right),\end{aligned} \quad (17)$$

where $\vec{n}$ is the outward unit normal at the boundary, B_h and B_c are the mass transfer coefficients, respectively, for the relative humidity and chloride (m/s), h_s and C_s are the relative humidity and free chloride concentration at concrete surface, h_{en} and C_{en} are the relative humidity and free chloride concentration at environment, and n is the environment factor, accounting for 1 during wetting and 0 during drying. Other values for the boundary condition are given in Table 1.

2.4. Input Parameters. To investigate the effects of the mix condition on the chloride penetration in nonsaturated concrete, 0.4, 0.5, and 0.6 of the water to cement ratio (w/c) were considered by using each porosity and pore size distribution, which were determined based on the mercury intrusion porosimetry (MIP). For the MIP test, mortar specimens with 0.4, 0.5, and 0.6 of w/c and 2.15 of the sand to cement ratio were fabricated using ordinary Portland cement (OPC). After water curing at $20 \pm 1^{\circ}C$ for 56 days, the samples were dried in an oven for 3 days to remove the inside pore solution. Then, mercury intrusion was implemented on the treated samples under a constant contact angle (130°). Mercury pressure was gradually increased up to 228 MPa, which then converted into the pore size distribution by using Washburn's equation. With the cumulative porosity data obtained from the MIP, B in (6) was determined with a nonlinear curve fitting method to the data. As for the effective chloride diffusivity, the values for 0.4, 0.5, and 0.6 of w/c were assumed to be 3.9, 7.8, and $12.6E-12\,m^2/s$ [17] which were then used in the chloride transport simulation. Other input parameters were assumed to be irrespective of w/c and are given in Table 2.

Table 2: Input parameters for the moisture and chloride transport simulations.

Property	Notation	Unit	Value
Moisture equilibria at 20°C	P_0	Pa	2333.4
	ρ_w	kg/m^3	994.6
	η	Pa·s	0.001
	l_m	m	$1E-7$
	γ	N/m	0.0728
	M_w	kg/mol	0.018
Chloride binding	α	—	1.15
	β	—	0.28
Surface transfer	B_h	m/s	$4.05E-7$
	B_c	m/s	$1.0E-6$

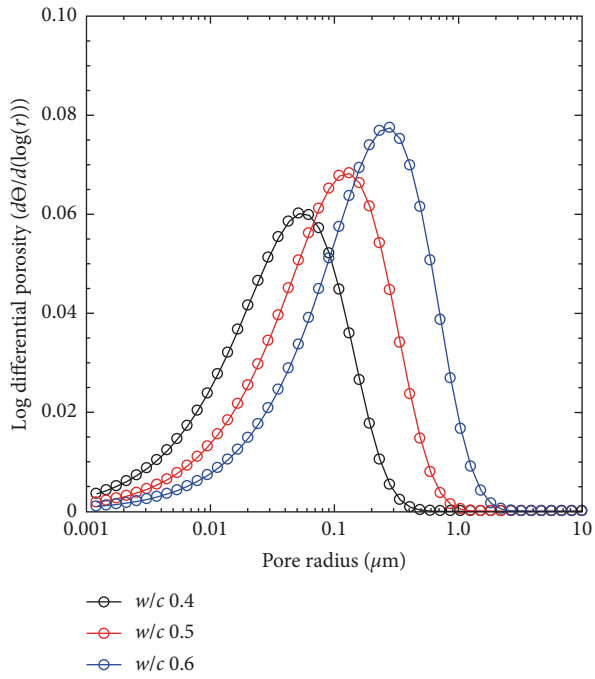

Figure 1: Pore size distributions with variation of water to cement ratios.

3. Result and Discussion

3.1. Pore Size Distribution. For the analysis of the combined moisture and chloride transport in concrete, pore size distribution depending on w/c was determined by regression analysis to the MIP data with R-R density function given in (6). As shown in Figure 1, the pore radius at maximum porosity increment increases with w/c, accounting for 0.051, 0.115, and 0.244 μm, respectively, for 0.4, 0.5, and 0.6 of w/c. In addition, porosity also increases with w/c, accounting for 0.16, 0.18, and 0.21. These observations indicate that the higher surplus of mixing water increases the portion of large capillary pores and water-filled porosity when concrete is saturated.

Based on the calculated pore size distribution, moisture adsorption and desorption isotherms can be determined using (12) and (13). As shown in Figure 2, the degree of saturation increases nonlinearly with the relative humidity,

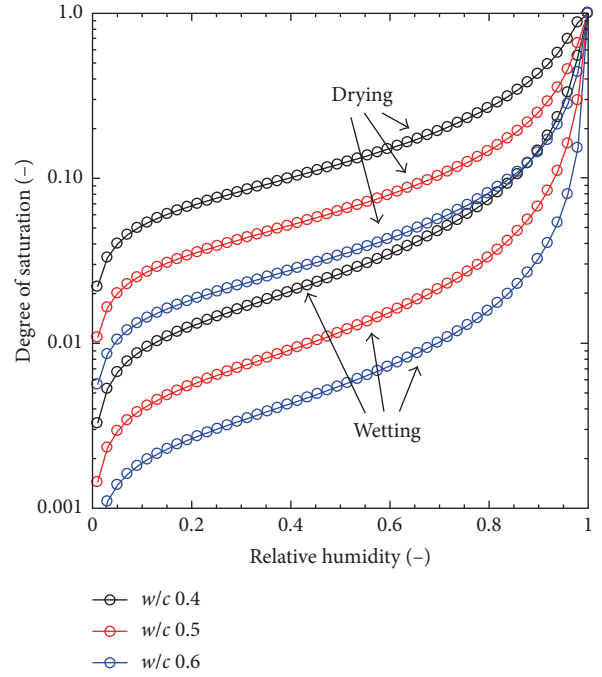

Figure 2: Moisture adsorption and desorption isotherms with variation of water to cement ratios.

and the difference in moisture level between wetting and drying always occurs due to the moisture entrapment through the ink-bottle pores. However, at given humidity level, degree of saturation decreases with w/c since the lower w/c leads to the higher portion of small capillary pores. This can imply that the higher the w/c is, the higher the amount of water content can be adsorbed during wetting or desorbed during drying.

3.2. Transport under Tidal Environment. To solve the nonlinear partial differential equations for the moisture and chloride transport, MATLAB PDE toolbox was used for the FEM analysis. Numerical calculation with convergence criteria (i.e., below 10^{-4}) was carried out on a two-dimensional rectangle domain with 4820 of the triangle mesh and 0.1 days of time step. Then, one-dimensional spatial values were obtained by interpolating the two-dimensional simulation results through a straight line from the concrete surface contacted with the ambient condition to the interior of material.

Due to the fluctuation of sea level in the tidal zone, moisture and chloride are transported into or out of the concrete surface to distort the concentration distributions with time. When the exposure condition changes from wetting to drying in the medium tide level, corresponding distributions of the moisture and chloride in concrete with 0.5 of w/c were calculated and depicted in Figure 3. As shown in Figure 3, the chloride profile at the end of wetting shows a steep increment in the concentration observed from the concrete surface to about 4 mm of depth below which the cover is nearly saturated. However, the chloride profile at the end of drying shows lower concentration increment up to

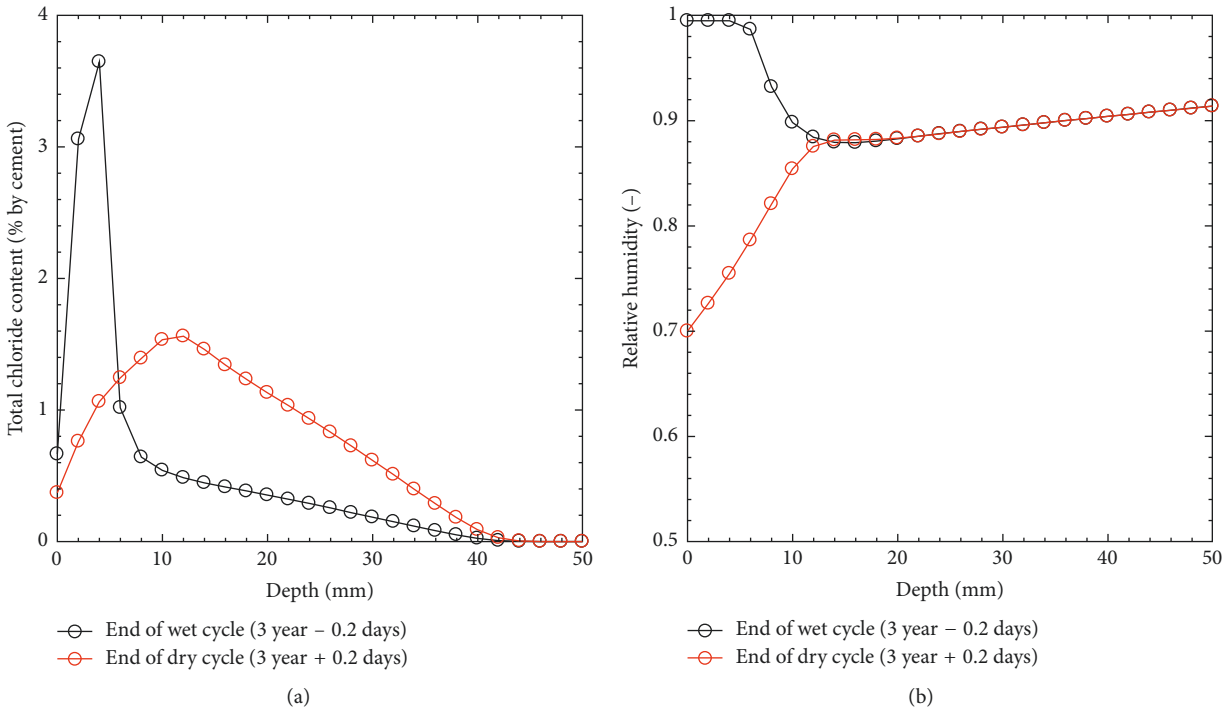

Figure 3: Change in concentration distributions of (a) chloride and (b) relative humidity during one cycle of drying process.

about 12 mm of depth below which moisture evaporation toward the concrete surface locally reduces the moisture content. Hence, the maximum chloride concentration accumulated near the concrete surface due to the wet/dry cycles is generated in the convection zone where the moisture intake during wetting and loss during drying repeatedly occur [18]. As shown in Figure 3(b), the convection zone ranges from the concrete surface to about 12 mm. However, over the convection zone, the chloride concentration generally decreases with the penetration depth and the variation of moisture level is relatively low. Thus, the convection zone occurs through the concrete depth up to the position at the peak value of the concentration generated after one cycle of drying. Simultaneously, the diffusion zone occurs from the end of the convection zone to inner concrete depth where the chloride transport is mostly governed by diffusion rather than convection [19]. Moreover, as shown in Figure 3(a), the chloride profile redistributed during drying always maintains higher concentration through the inner concrete depth since the higher concentration gradient in the convection zone generated during wetting could accelerate the ionic penetration into the diffusion zone during drying.

To investigate the influences of the tide level and mix condition on the chloride penetration in concrete, three types of daily drying time and w/c were reflected in the moisture and chloride profiles, respectively, as given in Figures 4 and 5. In these cases, 0.5 of w/c was used as a mix condition for the simulation in Figure 4, and the medium tide level was used as a boundary condition for the simulation in Figure 5.

As shown in Figure 4(a), the chloride profiles at the tidal zone show lower concentrations at the surface, accounting for 0.27–0.44% by cement which is about two times less than that for the submerged zone due to the diffusion into the sea water with lower concentration. However, the maximum concentrations accumulated at the interface between convection and diffusion zones exceed the surface concentration obtained in the submerged condition by about 1.3–2.5 times through 1–10 years, increasing with the tide level and exposure time. Specially, as the tide level increases, the concentration at 50 mm for 10 years increases from 0.45 to 0.74% by cement, which could lead to the higher risk of chloride-induced corrosion [20] as compared to that for the submerged condition. As shown in Figure 4(b), the maximum chloride concentration at the interface is shown to increase with the moisture evaporation rate from the inner concrete depth to the surface which is higher as the tide level increases. As the moisture evaporation rate increases at the same exposure time, more chloride sources can be accumulated at the interface due to the increase in nonsaturated porosity during drying [21] which can enhance the convective flow in concrete to draw out the chloride concentration in the diffusion zone to the convection zone at a higher rate. Consequently, chloride penetration in concrete is accelerated as tide level increases to elevate the concentration gradient toward the inner depth, despite little variation of water content through the diffusion zone.

As shown in Figure 5(a), chloride transport is highly dependent on w/c, revealing that as w/c increases, chloride concentration at the interface and the overall rate of ionic penetration increase at the same exposure time. For example, the maximum penetration depth for 0.4 of w/c increases from about 16 to 30 mm from 1 to 3 years while that for 0.6 of w/c increases from about 34 to over 50 mm for the

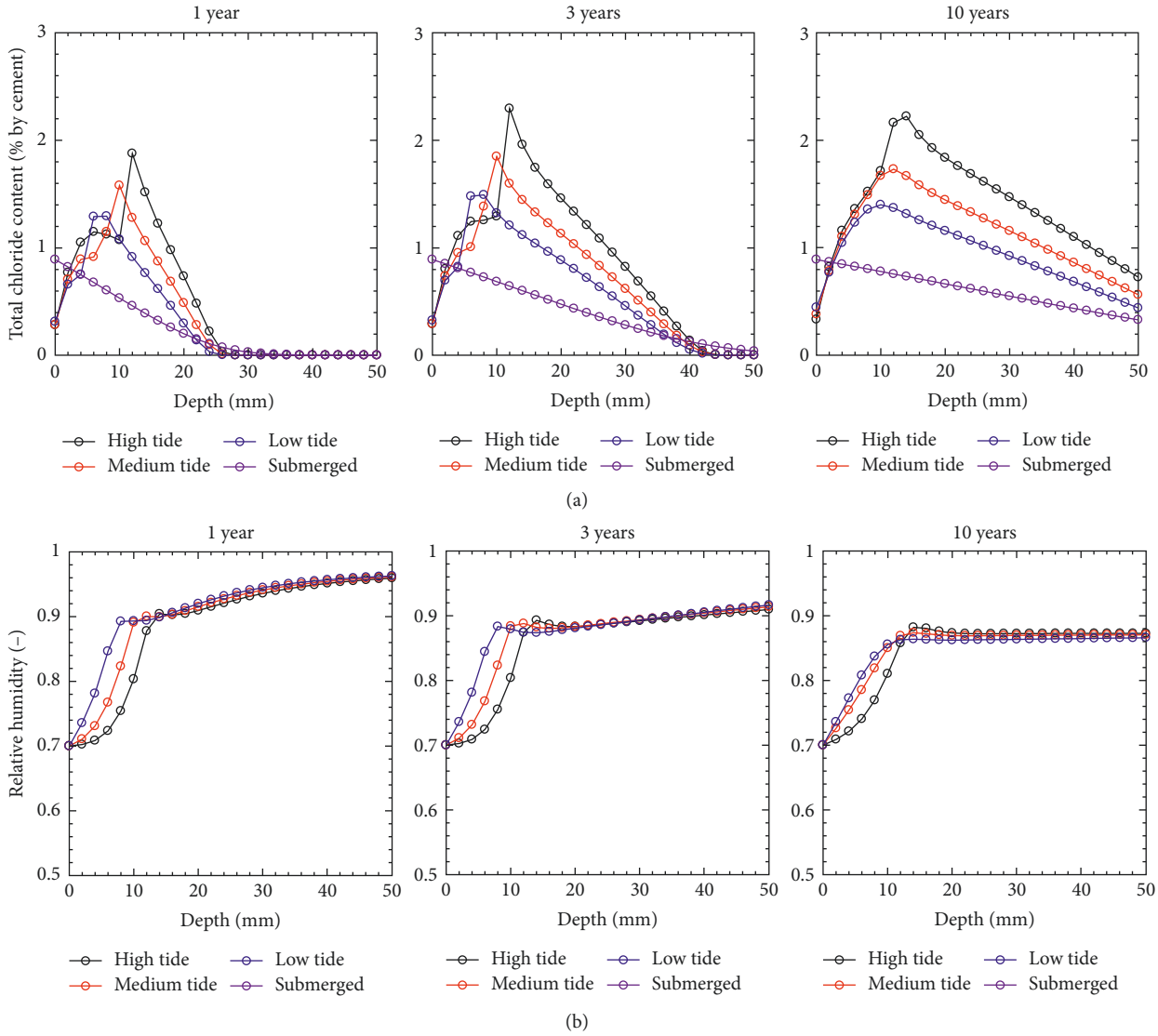

Figure 4: Concentration distributions of (a) chloride and (b) relative humidity depending on tide level at 0.5 of the water to cement ratio.

same period. In general, the higher w/c leads to the higher pore connectivity to decrease the tortuosity for the pathway of mass transfer in concrete [22]. According to (5), the tortuosity for 0.4, 0.5, and 0.6 of w/c was calculated to be 3.9, 3.2, and 2.9, respectively. Therefore, the increased moisture permeability arose from the decreased tortuosity could promote both the moisture permeation during wetting to allow more chloride source into the concrete and moisture evaporation during drying to enhance the concentration buildup at the interface. Simultaneously, the fraction of large capillary pores generally increases with w/c, as indicated in Figure 1, which can also elevate the ionic diffusion rate [23] due to the large increase in the water-filled porosity through inner concrete depth. As shown in Figure 5(b), moisture level over the diffusion zone for 0.6 of w/c is always higher than that for 0.4 of w/c, implying that the higher rate of chloride diffusion due to the increased water filled porosity as well as the effective chloride diffusivity could enhance the overall ionic penetration in nonsaturated concrete.

3.3. Service Life Assessment. To relate the influential factors (i.e., tide level and w/c) to the service life of RC structures built in tidal environment, the maximum chloride concentration at the interface, which largely depends on those factors, was calculated and is depicted in Figure 6. Then, by relating the maximum concentration to the onset of chloride-induced corrosion, sensitivity analysis for designing the minimum required cover depth was carried out on those factors, which are depicted in Figure 7. In this case, the steel corrosion in concrete was assumed to initiate at which the chloride threshold level (CTL) reaches the steel embedded depth (i.e., cover depth). For the CTL, 0.4% by cement as a total chloride content [24] was used to all the simulations since a large variation in the value, depending on the detection method and chloride exposure condition, has been reported [20].

As shown in Figure 6, all the maximum chloride concentrations were determined at drying with 10 days of increments since more chloride sources penetrate into the

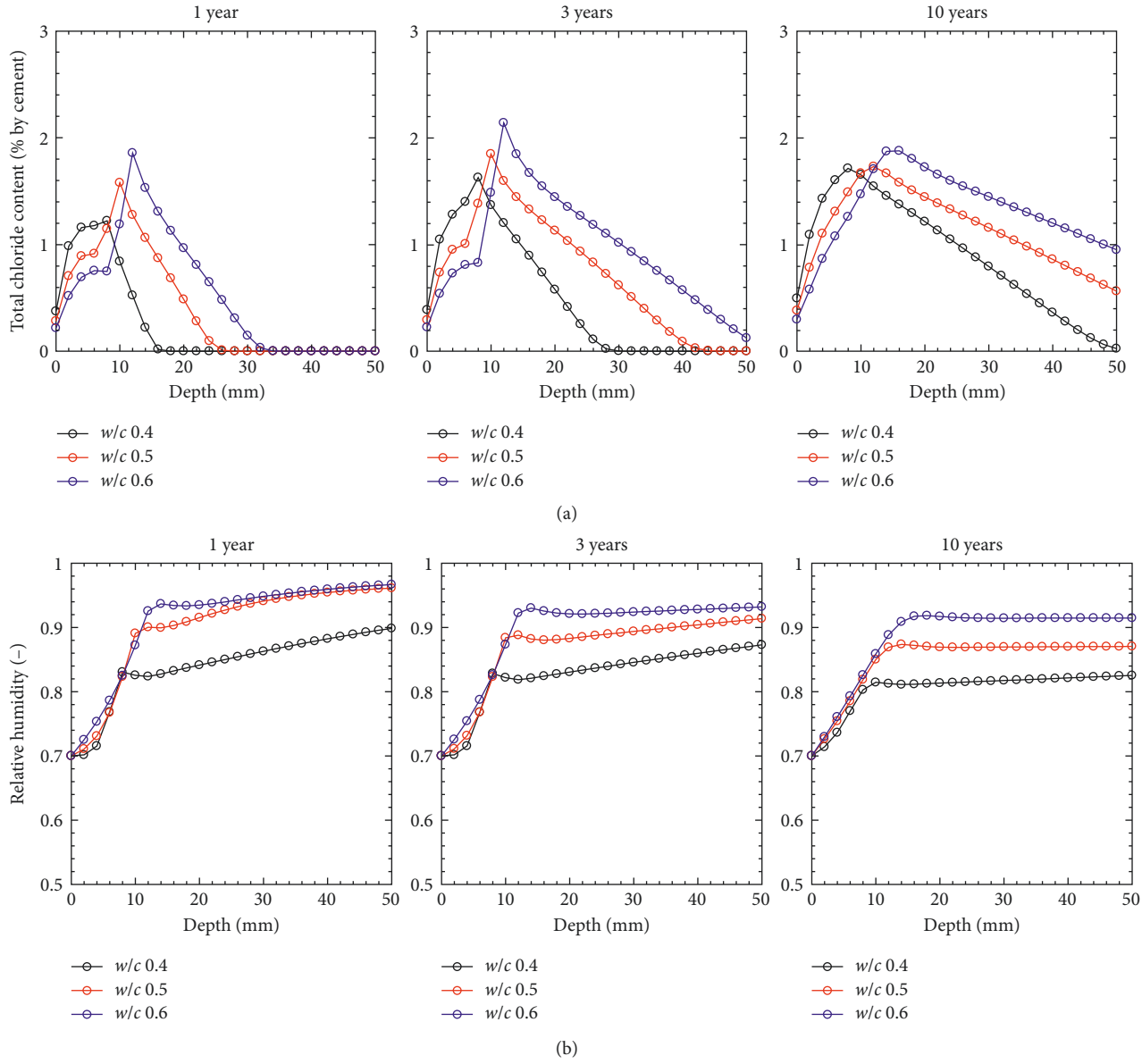

Figure 5: Concentration distributions of (a) chloride and (b) relative humidity depending on mix condition at medium tide level.

inner concrete depth after one cycle of wetting, as indicated in Figure 3(a). As shown in Figure 6(a), chloride concentrations at the interface are distinctively increased with tide level at the same exposure time while in Figure 6(b), the concentration evolution depending on w/c is less significant. For example, at 10 years of exposure time, the concentration from the low to high tide increases from 1.6 to 2.3% by cement, while that from the 0.4 to 0.6 of w/c only increases from 1.8 to 2.1% by cement. Hence, the convective chloride transport is more significant as the tide level increases than the variation of w/c.

As shown in Figure 7, the minimum required cover depth, defined as the depth with the CTL (i.e., 0.4% by cement), generally increases with the maximum chloride concentration through all the factors. However, the increasing rate of cover depth highly depends on the maximum concentration at the interface. Before reaching about 1.2–1.8% by cement, the cover depth in Figure 7(a) increases proportionally with the concentration and then increases notably while the transient increase in the cover depth in Figure 7(b) starts to occur at about 1.4–1.6% by cement. The chloride concentration at the transient increase of the cover depth would be the one at which the chloride buildup at the interface becomes marginal with time, generally observed over 1–2 years in Figure 6. Thus, it can be inferred that after a certain amount of chloride accumulate at the interface, chloride diffusion would control the overall transport rate due to the large concentration gradient, which are more sensitive to w/c than tide level. In fact, as shown in Figure 7(b), the required cover depth for 10 years exposure to the medium tide level increases from 41.3 to 71.8 mm as w/c increases from 0.4 to 0.6, while at the same time and mix condition (i.e., 0.5 w/c), the increment in the

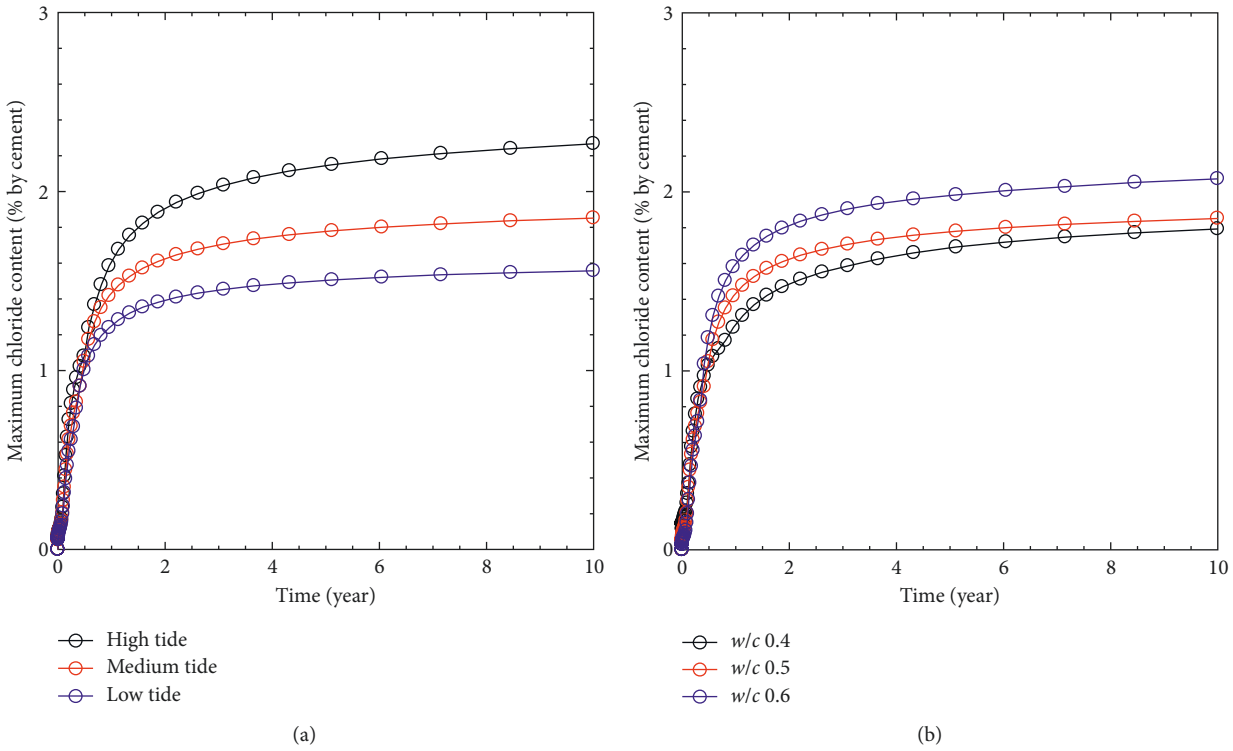

Figure 6: Concentration buildup at the interface between convection and diffusion zones depending on (a) tide level and (b) water to cement ratio.

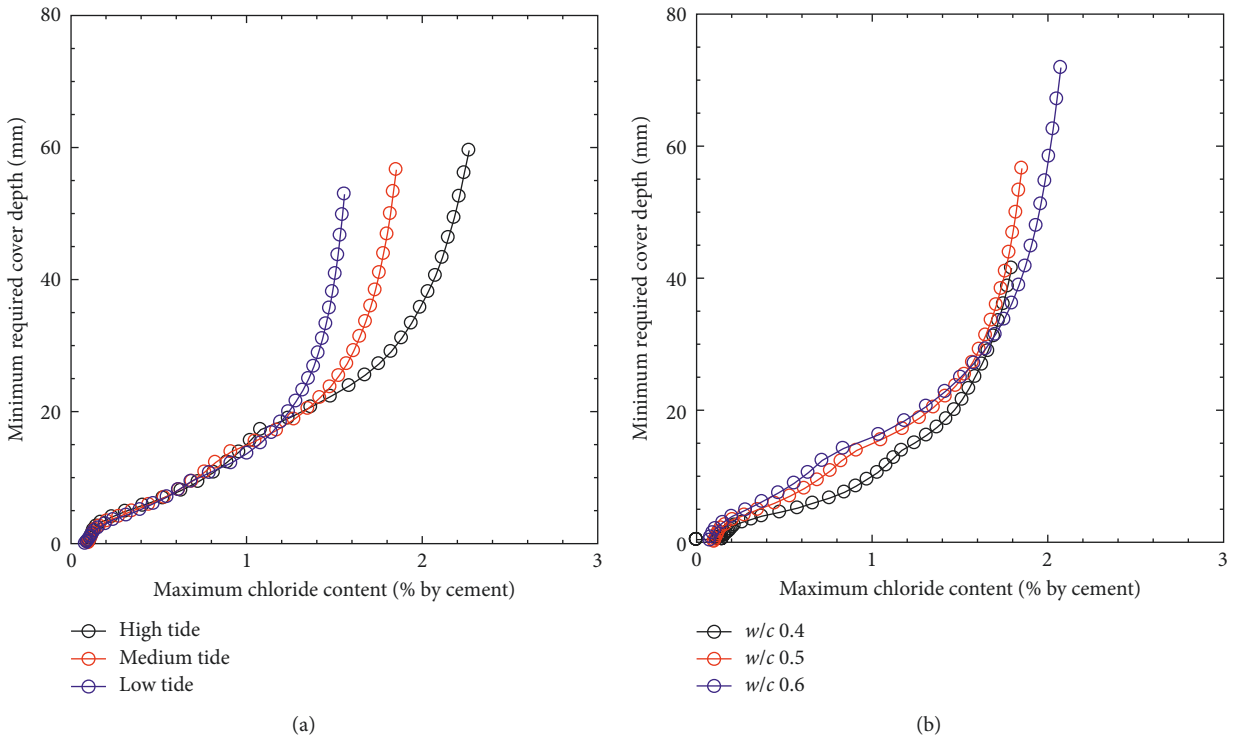

Figure 7: Minimum required cover depth against chloride-induced corrosion depending on (a) tide level and (b) water to cement ratio.

cover depth in Figure 7(a) shows a little variation from 52.9 to 59.6 mm with the tide level. Hence, to enhance the durability of RC structures built in the tidal environment, lowering w/c is primarily recommended otherwise regular maintenance, for example, using the technique of electrochemical chloride removal [25], to reduce the chloride content accumulated at the interface may be essential.

4. Conclusion

The present study aims to assess the service life of concrete structures exposed to the tidal zone with the proposed numerical model for predicting the moisture and chloride transport in concrete. As the influential factors of the service life, three types of daily wet/dry durations in the tidal zone and water to cement ratios in concrete mix were considered in the simulation. From the result, the following conclusion was drawn:

(1) Pore size distribution, obtained by fitting the R-R density function to the cumulative porosity data in the MIP, was used to determine the moisture permeability and degree of saturation in nonsaturated concrete. Based on the pore size distribution, it was found that the higher w/c in concrete mix leads to the higher portion of large capillary pores and the lower degree of saturation at given humidity level.

(2) Moisture and chloride distribution in concrete with variations of the tide level and w/c was calculated over 10 years of exposure period. As the tide level increases, the moisture evaporation rate toward the concrete surface increases to promote the chloride buildup at the interface between convection and diffusion zones and increases the rate of chloride penetration into the concrete cover at the same exposure time. Similarly, as w/c increases, the maximum chloride concentration at the interface increases and simultaneously the rate of diffusion increases due to the higher effective chloride diffusivity and water-filled porosity, thereby increasing the ionic penetration depth at the same exposure time.

(3) Sensitivity analysis of the service life to the tide level and w/c was carried out on the calculated chloride profiles over 10 years of exposure time. As a result, the required cover depth at which the CTL reaches on the steel embedment generally increases with the maximum concentration at the interface while the rate of increase in the cover depth with concentration is much higher when the w/c increases from the lowest to the highest, as compared with those for the tide level.

Conflicts of Interest

The authors declare that they have no conflicts of interest.

Acknowledgments

This research was supported by Technology Advancement Research Program funded by Ministry of Land, Infrastructures and Transport of Korean Government (Grant no. 17CTAP-C097546-03).

References

[1] C. L. Page, "Mechanism of corrosion protection in reinforced concrete marine structures," *Nature*, vol. 258, no. 5535, pp. 514-515, 1975.

[2] A. M. Neville, *Properties of Concrete*, Longman Group, London, UK, 4th edition, 1995.

[3] H.-W. Song, C.-H. Lee, and K. Y. Ann, "Factors influencing chloride transport in concrete structures exposed to marine environments," *Cement and Concrete Composites*, vol. 30, no. 2, pp. 113–121, 2008.

[4] M. D. A. Thomas and P. B. Bamforth, "Modelling chloride diffusion in concrete: effect of fly ash and slag," *Cement and Concrete Research*, vol. 29, no. 4, pp. 487–495, 1999.

[5] S.-W. Pack, M.-S. Jung, H.-W. Song, S.-H. Kim, and K. Y. Ann, "Prediction of time dependent chloride transport in concrete structures exposed to a marine environment," *Cement and Concrete Research*, vol. 40, no. 2, pp. 302–312, 2010.

[6] M. K. Moradllo, M. Shekarchi, and M. Hoseini, "Time-dependent performance of concrete surface coatings in tidal zone of marine environment," *Construction and Building Materials*, vol. 30, pp. 198–205, 2012.

[7] A. Da Costa, M. Fenaux, J. Fernández, E. Sánchez, and A. Moragues, "Modelling of chloride penetration into non-saturated concrete: case study application for real marine offshore structures," *Construction and Building Materials*, vol. 43, pp. 217–224, 2013.

[8] A. V. Saetta, R. V. Scotta, and R. V. Vitaliani, "Analysis of chloride diffusion into partially saturated concrete," *Materials Journal*, vol. 90, no. 5, pp. 441–451, 1993.

[9] B. Martin-Pérez, S. Pantazopoulou, and M. Thomas, "Numerical solution of mass transport equations in concrete structures," *Computers and Structures*, vol. 79, no. 13, pp. 1251–1264, 2001.

[10] E. P. Nielsen and M. R. Geiker, "Chloride diffusion in partially saturated cementitious material," *Cement and Concrete Research*, vol. 33, no. 1, pp. 133–138, 2003.

[11] H. Sleiman, O. Amiri, A. Ait-Mokhtar, and J.-M. Loche, "Chloride transport through unsaturated concrete: chloride profile simulations and experimental validation," *Magazine of Concrete Research*, vol. 64, no. 4, pp. 351–359, 2012.

[12] Q. Huang, Z. Jiang, X. Gu, W. Zhang, and B. Guo, "Numerical simulation of moisture transport in concrete based on a pore size distribution model," *Cement and Concrete Research*, vol. 67, pp. 31–43, 2015.

[13] R. Chaube, T. Kishi, and K. Maekawa, *Modelling of Concrete Performance: Hydration, Microstructure and Mass Transport*, CRC Press, New York, NY, USA, 2005.

[14] K. Nakarai, T. Ishida, and K. Maekawa, "Multi-scale physicochemical modeling of soil-cementitious material interaction," *Soils and Foundations*, vol. 46, no. 5, pp. 653–663, 2006.

[15] H. Ranaivomanana, J. Verdier, A. Sellier, and X. Bourbon, "Toward a better comprehension and modeling of hysteresis cycles in the water sorption–desorption process for cement based materials," *Cement and Concrete Research*, vol. 41, no. 8, pp. 817–827, 2011.

[16] D. Quenard and H. Sallee, "Water vapour adsorption and transfer in cement-based materials: a network simulation," *Materials and Structures*, vol. 25, no. 9, pp. 515–522, 1992.

[17] V. Ngala, C. Page, L. J. Parrott, and S. Yu, "Diffusion in cementitious materials: II, further investigations of chloride and oxygen diffusion in well-cured OPC and OPC/30% PFA pastes," *Cement and Concrete Research*, vol. 25, no. 4, pp. 819–826, 1995.

[18] K. Li, C. Li, and Z. Chen, "Influential depth of moisture transport in concrete subject to drying–wetting cycles," *Cement and Concrete Composites*, vol. 31, no. 10, pp. 693–698, 2009.

[19] C. Andrade, M. Climent, and G. de Vera, "Procedure for calculating the chloride diffusion coefficient and surface concentration from a profile having a maximum beyond the concrete surface," *Materials and Structures*, vol. 48, no. 4, pp. 863–869, 2015.

[20] K. Y. Ann and H.-W. Song, "Chloride threshold level for corrosion of steel in concrete," *Corrosion Science*, vol. 49, no. 11, pp. 4113–4133, 2007.

[21] H. Chang, S. Mu, D. Xie, and P. Wang, "Influence of pore structure and moisture distribution on chloride "maximum phenomenon" in surface layer of specimens exposed to cyclic drying-wetting condition," *Construction and Building Materials*, vol. 131, pp. 16–30, 2017.

[22] L. Liu, W. Sun, G. Ye, H. Chen, and Z. Qian, "Estimation of the ionic diffusivity of virtual cement paste by random walk algorithm," *Construction and Building Materials*, vol. 28, no. 1, pp. 405–413, 2012.

[23] N. Olsson, V. Baroghel-Bouny, L.-O. Nilsson, and M. Thiery, "Non-saturated ion diffusion in concrete–a new approach to evaluate conductivity measurements," *Cement and Concrete Composites*, vol. 40, pp. 40–47, 2013.

[24] British Standard, *Structural Use of Concrete: Code of Practice for design and Construction, BS 8110*, British Standard Institute, London, UK, 1985.

[25] Y. Wang, L. Li, and C. Page, "A two-dimensional model of electrochemical chloride removal from concrete," *Computational Materials Science*, vol. 20, no. 2, pp. 196–212, 2001.